PROCEEDINGS A

rspa.royalsocietypublishing.org

Research

Article submitted to journal

Subject Areas:
xxxxx, xxxxx, xxxx

Keywords:
auxetic, phase transforming, bifurcation, complex system, emergence

Author for correspondence:
Giles W Hunt
e-mail: g.w.hunt@bath.ac.uk

THE ROYAL SOCIETY
PUBLISHING

Complexity in Phase Transforming Pin-Jointed Auxetic Lattices

G. W. Hunt[1] and T. J. Dodwell[2,3]

[1]Department of Mechanical Engineering, University of Bath, Bath BA2 7AY, UK.
[2]College of Engineering, Mathematics & Physical Sciences, University of Exeter, Exeter EX4 4PY, UK.
[3]The Alan Turing Institute, London, NW1 2DB, UK.

We demonstrate the complexity that can exist in the modelling of auxetic lattices. By introducing pin-jointed members and large deformations to the analysis of a re-entrant structure, we create a material which has both auxetic and non-auxetic phases. Such lattices exhibit complex equilibrium behaviour during the highly nonlinear transition between these two states. The local response is seen to switch many times between stable and unstable states, exhibiting both positive and negative stiffnesses. However, there is shown to exist an underlying *emergent modulus* over the transitional phase, to describe the average axial stiffness of a system comprising a large number of cells.

1. Introduction

Auxetic materials are both intriguing and compelling, in that they break our physical intuition of a material. When uniaxially stretched (compressed), they expand (contract) laterally. This counter-intuitive, emergent response, is driven by the geometric arrangement of the small-scale structure of the material. Various microscale arrangements exhibit auxetic mechanics. The most common studied is the re-entrant structure [1–3] as shown in Fig. 2. Properties of these materials typically exhibit high energy absorption and fracture resistance, and hence have a broad range of practical applications from: blast curtains, shock absorbers to running trainers. See for example [1–9] and references therein.

In this paper demonstrate the underlying complexity which is uncovered with a simple alteration to the standard re-entrant structure, by allowing the connections between members to be pin-jointed. When exploring the large deformation behaviour of the unit cell Fig. 2, the

arrangement exhibits a complex transition between auxetic and non-auxetic phases. When scaled up to an array of such unit cells, as shown in Fig. 5, the complex behaviour has much in common with so-called *snaking behaviour* [10], with an added complication that equilibrium solutions fluctuate not just in load, but also in the corresponding deflection of the load. Consequently, such behaviour can justifyingly be termed complex.

One of the key characteristics of a complex system is that it should exhibit *emergent properties*, that can be identified on the system as a whole [11,12], but not necessarily on a local level. We focus here on homogeneity (or otherwise) in auxetic materials modelling. For the systems of interest, we find an *emergent axial stiffness* for the global response, which is not immediately obvious from the local behaviour of the cells themselves.

The paper starts with the response of a single-cell model comprising two simple arch elements connected by a single coupling spring. This exhibits both auxetic and non-auxetic phases. While both phases are symmetric, in the sense that the two degrees of freedom displace by the same amount, such states are unstable during transition. The stable route breaks this symmetry, with the two components of the cell displacing in turn rather than simultaneously. Analysis is then extended to multiple cells acting in parallel, and finally into such tiers of cells acting in series, where the full complexity of possible behaviour becomes apparent.

2. Single Cell Formulation

Before discussing the cell of Fig. 2, it is useful first to review the response of its forerunner, the simple tied arch of Fig. 1. Total potential energy of this well-known single-degree-of-freedom

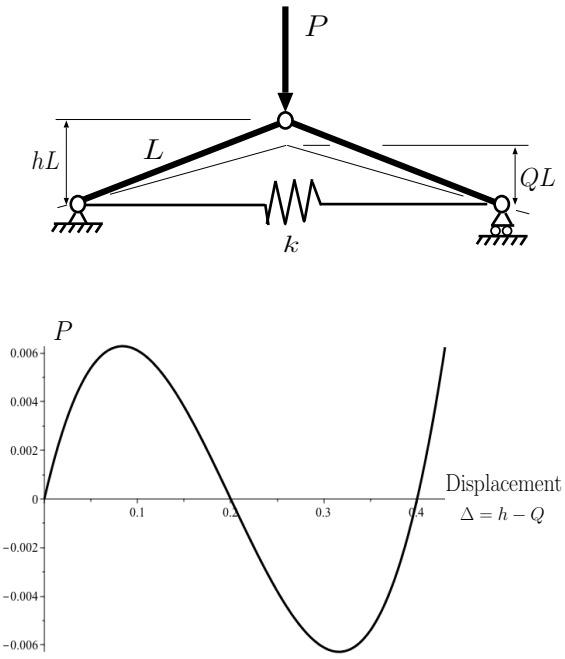

Figure 1. Single degree of freedom tied arch model and its response under load P for $L = 1$ $h = 0.2$ and $k = 1$. The spring is unstressed when $P = 0$ and $Q = h$.

system (see for example [13], p.61), comprising strain energy minus work done by the load P moving through its corresponding displacement Δ, where $\Delta = h - Q$, is given by

$$V = \frac{1}{2}kL^2\left(2\sqrt{1-h^2} - 2\sqrt{1-Q^2}\right)^2 - PL(h-Q), \tag{2.1}$$

with equilibrium states determined from the single nonlinear equation $dV/dQ = 0$. The response is as shown. Starting from the illustrated state, under positive load P the arch starts to flatten, with stiffness dropping off and eventually falling to zero as the equilibrium path reaches its maximum. A falling equilibrium path then follows, unstable under load control (dead load) but stable if displacement is controlled as is the case in many buckling experiments [14]. The load itself eventually drops to zero as the arch reaches the totally flat configuration. Following this, with load reversed, the equilibrium path passes through a minimum before the load eventually drops to zero again as the arch reaches its fully inverted state.

Fig. 2 shows a typical cell used to model auxetic material behaviour [1–3]. Two arches like that

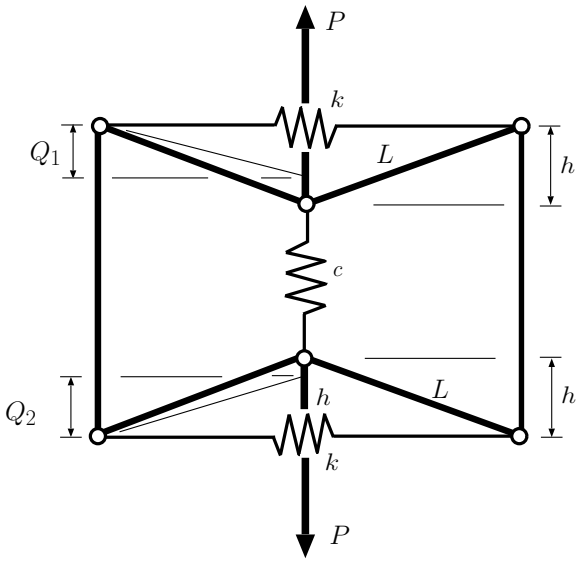

Figure 2. A model for an auxetic cell. The position shown is in the auxetic configuration, switching to non-auxetic once the arms have passed through horizontal. Typically, the arches snap through in turn rather than simultaneously.

of Fig. 1 are placed back to back and coupled by a spring of stiffness c. Under tensile load (positive P), the arches tend to flatten, causing the cell initially to expand in the direction perpendicular to the loading. Note that when they have gone beyond flat the cell will start to contract, thus entering a non-auxetic phase. Coupling spring energy is determined from the sum of displacements $h - Q_1$ and $h - Q_2$, and so with all springs unstressed when $Q_1 = Q_2 = h$, the total potential energy is given by

$$\begin{aligned} V = &\frac{1}{2}kL^2\left(2\sqrt{1-h^2} - 2\sqrt{1-Q_1^2}\right)^2 + \frac{1}{2}kL^2\left(2\sqrt{1-h^2} - 2\sqrt{1-Q_2^2}\right)^2 \\ &+\frac{1}{2}cL^2\left(2h - Q_1 - Q_2\right)^2 - PL\left(2h - Q_1 - Q_2\right). \end{aligned} \tag{2.2}$$

The first two terms represent the strain energy in the horizontal springs, the third is the strain energy of the (coupling) vertical spring, and the final term is the work done by load P moving through its corresponding displacement, Δ;

$$\Delta = L\left(2h - Q_1 - Q_2\right). \tag{2.3}$$

Equilibrium states can be found from the two equilibrium equations $\partial V/\partial Q_1 = 0$ and $\partial V/\partial Q_2 = 0$, while stability under controlled displacement Δ can be determined by examining the sign of the determinant of $\partial^2 V/\partial Q_{ij}^2$ using (2.3) as a constraint equation with P acting as a Lagrange

multiplier. Such analysis is readily performed using the algebraic manipulation program Maple™ [15].

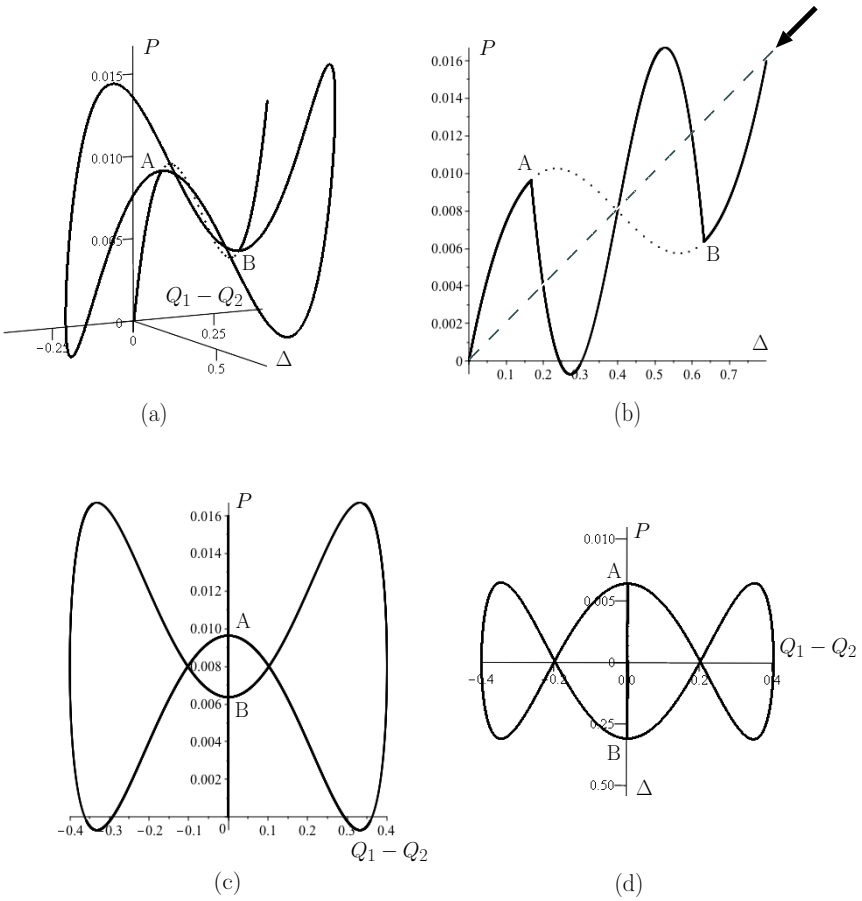

Figure 3. Response of the cell of Fig.2 for $L = 1, h = 0.2, k = 1$ and $c = 0.02$. Solid lines depict stable equilibrium states under controlled stretch Δ, and the dotted line unstable states. (a) Three dimensional plot of load P against its corresponding deflection Δ and the symmetry-breaking variable $(Q_1 - Q_2)$. (b) Projection onto the $P - \Delta$ plane. (c) Projection onto the $P - (Q_1 - Q_2)$ plane. (d) Projection onto plane perpendicular to the direction of the arrow in (b).

A typical equilibrium response is shown in Fig. 3, on a three-dimensional plot of load P against its corresponding displacement Δ and the symmetry-breaking variable $(Q_1 - Q_2)$ in (a), and projected onto three different planes in (b), (c) and (d). The response starts from zero load with positive stiffness and is homogeneous $(Q_1 = Q_2)$, continuing up and over a limit point [14] where the stiffness becomes negative. This path reflects the behaviour of the related one degree-of-freedom tied arch of Fig. 1. But before this first limit point is reached, at bifurcation point A the homogeneous solution becomes unstable. Under controlled load, both arches would then suddenly snap through, and the system would eventually re-stabilise at the same load level on the stable path above B. If displacement Δ is the controlled parameter however, at bifurcation point A stability switches to the non-homogeneous $(Q_1 \neq Q_2)$ solution. This secondary path performs a loop under fluctuating load, during which one of the constituent arches and then the other pass through their flat configurations, and eventually re-engages with the homogeneous path at a second bifurcation point B where stability transfers back. As seen in Fig. 3(b), during this process the effective stiffness of the system is constantly changing, positive but falling up to A,

switching to negative then positive then negative again until B, and finally turning positive and stiffening further after B. The transformation of the cell from the auxetic phase (before A) to the non-auxetic (after B) is thus seen to be a relatively complex process, taking place over a finite (non-homogenous) displacement range between the two bifurcations. We note that this switching of stability from homogeneous to non-homogeneous state with the stiffness remaining positive runs counter to other simple systems sometimes used to describe the localisation process [10,16], in which homogeneity is breached only after a maximum on an equilibrium path is reached.

The dashed line indicates the path that would be followed by the linear coupling spring alone, without the nonlinear effects of the two arches. We see that this runs right up the middle of the actual response, effectively averaging out the nonlinear effects. This characteristic extends into the multiple cells which follow, and is the basis of the concept of *emergent stiffness*, is explained in more detail in §5.

Fig. 4 shows the response of the cell of Fig. 2 for different values of the coupling spring stiffness

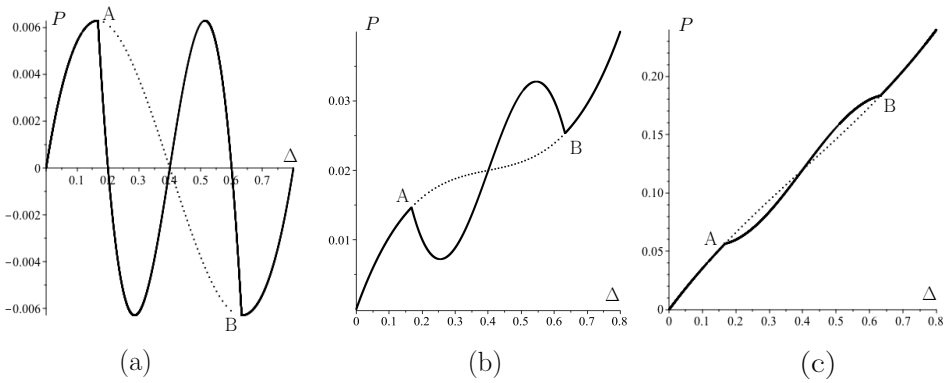

Figure 4. Load to corresponding deflection plots for the cell of Fig. 2 for different stiffnesses of coupling spring. a) $c = 0$. b) $c = 0.05$. c) $c = 0.5$.

c. For case (a) of $c = 0$, the same response of the arch of Fig. 1 is reproduced, with a significant difference that the homogeneous solution becomes unstable between the two bifurcation points A and B, which now coincide with the maximum and minimum states on the path at *hill-top branching points* [13]. We see that the non-homogeneous equilibrium path is retained for all examined situations, but for the high value of c, in this particular projection, it remains close to the homogeneous solution. It is interesting to observe that a line drawn between the unloaded state where $Q_1 = Q_2 = h$ and $\Delta = 0$, and its inverse at $Q_1 = Q_2 = -h$ and $\Delta = 4h = 0.8$ (the dashed line of Fig. 3(b)) again reproduces the response of the coupling spring on its own. We shall return to this point in the emergent stiffness discussion of §5.

3. Multiple Cells

The single cell of Fig. 2 can be extended both horizontally and vertically as seen in Fig. 5. As shown, each row of $N(=4)$ rigid links has $N-1$ horizontal springs and either $N/2$ upper pins and $N/2+1$ lower pins, or vice versa. With each pin connecting to a vertical spring, each row of the latter therefore has either $N/2$ or $N/2+1$ members. As $N \to \infty$, $N-1$ and $N+1 \to N$, and with reference to (2.2) the strain energy U stored in the springs of the general ith row simply becomes

$$U = \frac{1}{2}NkL^2\left(2\sqrt{1-h^2} - 2\sqrt{1-Q_i^2}\right)^2 + \frac{1}{4}NcL^2\left(2h - Q_{i+1} - Q_i\right)^2. \tag{3.1}$$

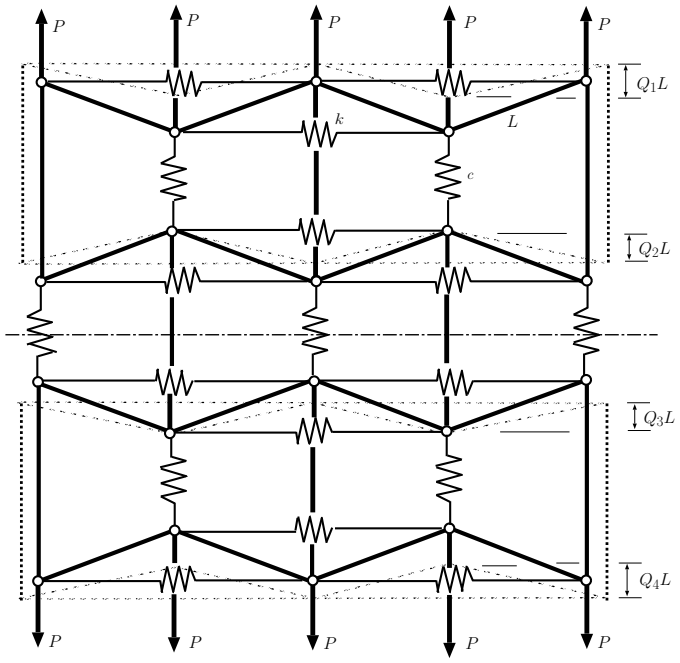

Figure 5. Combined cells of the form of Fig.2. With the centreline held stationary, displaced states are shown dashed. We refer to this configuration as a three-tier system and note that it has four effective degrees of freedom Q_i, $i = 1..4$.

Over n rows of links and finite but large width N we would therefore have

$$U = \frac{1}{2}NkL^2\sum_{i=1}^{n}\left(2\sqrt{1-h^2}-2\sqrt{1-Q_i^2}\right)^2+\frac{1}{4}NcL^2\sum_{i=1}^{n-1}\left(2h-Q_{i+1}-Q_i\right)^2. \tag{3.2}$$

For the work done by the load P, by referring to Fig. 5, it can be seen that upwards displacement of the top two load arrows adjacent to the middle equals the deflection $2h - Q_1 - Q_2$ in vertical springs directly below. However, because of the relative differences in displacement in the top row of pins, the middle arrow and the two outer ones move by just $h - Q_2$. In general, each internal row therefore provides a contribution towards the movement of the loads of $(h - Q_i)$ at all points of application, but the end rows provide this over just half of these positions. The total work done (WD) by the loads P over large width N and n rows can thus be written

$$WD = \frac{1}{2}NPL\left(h-Q_1\right)+NPL\sum_{i=2}^{n-1}\left(h-Q_i\right)+\frac{1}{2}NPL\left(h-Q_n\right), \tag{3.3}$$

as $N \to \infty$. Dividing throughout by N, we can therefore write the total potential energy function, $V = U - WD$, as

$$\begin{aligned} V =& \frac{1}{2}kL^2\sum_{i=1}^{n}\left(2\sqrt{1-h^2}-2\sqrt{1-Q_i^2}\right)^2+\frac{1}{4}cL^2\sum_{i=1}^{n-1}\left(2h-Q_{i+1}-Q_i\right)^2 \\ &-\frac{1}{2}PL\left(h-Q_1\right)-PL\sum_{i=2}^{n-1}\left(h-Q_i\right)-\frac{1}{2}PL\left(h-Q_n\right). \end{aligned} \tag{3.4}$$

Comparing the summed terms with their counterparts in the V-function (2.2) for a single cell, we see a difference in the coefficient for the coupling spring, which now $1/4$ instead $1/2$, and for P which likewise is halved. This means that, to enable direct stiffness and effective Young's modulus comparisons with the responses for a single cell, shown in Fig. 3, it is useful to note that

a single tier of cells involving two rows of arches would give these same plots if $L=1$, $h=0.2$, $k=0.5$ and $c=0.02$. These parameter values are used for all the multiple tier responses which follow.

Again, although the load positions move by two different amounts, for the purposes of the comparative plots the corresponding displacement of the load is taken to be

$$\Delta = L\,(h-Q_1) + 2L\sum_{i=2}^{n-1}(h-Q_i) + L\,(h-Q_n)\,, \tag{3.5}$$

representing the movement of the loading points adjacent to the middle position of Fig. 5.

(a) Two tiers ($n=3$)

Solutions to the three equilibrium equations $\partial V/\partial Q_i = 0, i=1..3$, where V is given by (3.4), are readily found using a standard Newton-Raphson scheme, with the outcomes shown in Fig. 6. These projections can be compared those of Fig. 3, with the difference in the parameter value of k noted above and the symmetry-breaking variable (Q_1-Q_3) replacing its counterpart (Q_1-Q_2).

With two tiers of cells the response is considerably more complex than for a single cell. There is now no specific homogeneous solution $Q_1=Q_2=Q_3$, but the same role is taken by the symmetric solution about the horizontal centreline for which $Q_1=Q_3$. This path fluctuates with P like the homogeneous solution of Fig. 3 but, unlike the latter, also reverses its direction with respect to Δ, so that it moves both backwards and forwards in Δ over the transition between auxetic and non-auxetic phases. This is shown in Fig. 6(b). As with the single cell, bifurcations A and B into non-symmetric solutions also occur. However, unlike the single cell, stability is lost completely at A, so on reaching this state under controlled Δ the system would then snap dynamically to one of the competing stable states that exist for lower values of P at the same Δ value. Figure 6(d) shows the locus of all equilibrium states when viewed in the direction of emergent stiffness, given by the arrow shown in (c).

(b) Three tiers (n=4)

It is of course not surprising that adding a third tier increases the complexity of the response, as is seen in Fig. 7. Plotting the three dimensions of load P against its corresponding deflection Δ and symmetry-breaking variable (Q_1-Q_4) gives the contorted set of paths shown in (a). Note that a second choice of symmetry-breaking variable could now be (Q_2-Q_3), resulting in a different but equally contorted set of equilibrium paths, not shown here. Equilibria that are symmetric about the horizontal centre line of Fig. 5, such that $Q_1=Q_4$ and $Q_2=Q_3$, are shown in (b). This has much the same form as Fig. 6(b), except for the fact that the number of bifurcations into non-symmetric states, where stability is either lost or regained with increasing Δ, has now increased from two to six. These points are marked as B on the plot, and suggest that the number of non-symmetric loops of equilibria has increased from one to three. The remaining plots show a selection of projections of the full behaviour on to various planes. These include that of Fig. 7(f), perpendicular to the direction shown in the arrow and compared later in §5 with those of Figs. 6(d) and 3(d).

(c) Four tiers (n=5)

We conclude this sequence of increasing complexity with the four-tier response of Fig. 8. This shows a similar set of plots to the three-tier example of Fig. 7, with a difference that (a), (d), (e) and (f) now exclusively use (Q_2-Q_4) as the choice of symmetry-breaking variable. Again it is noted that if (Q_1-Q_5) had been chosen, a different but similarly contorted set of projections would result. We see a further increase in complexity, it now being hard to distinguish the individual paths on the three-dimensional plot of (a). The symmetric path plot of Fig. 8(b) shows

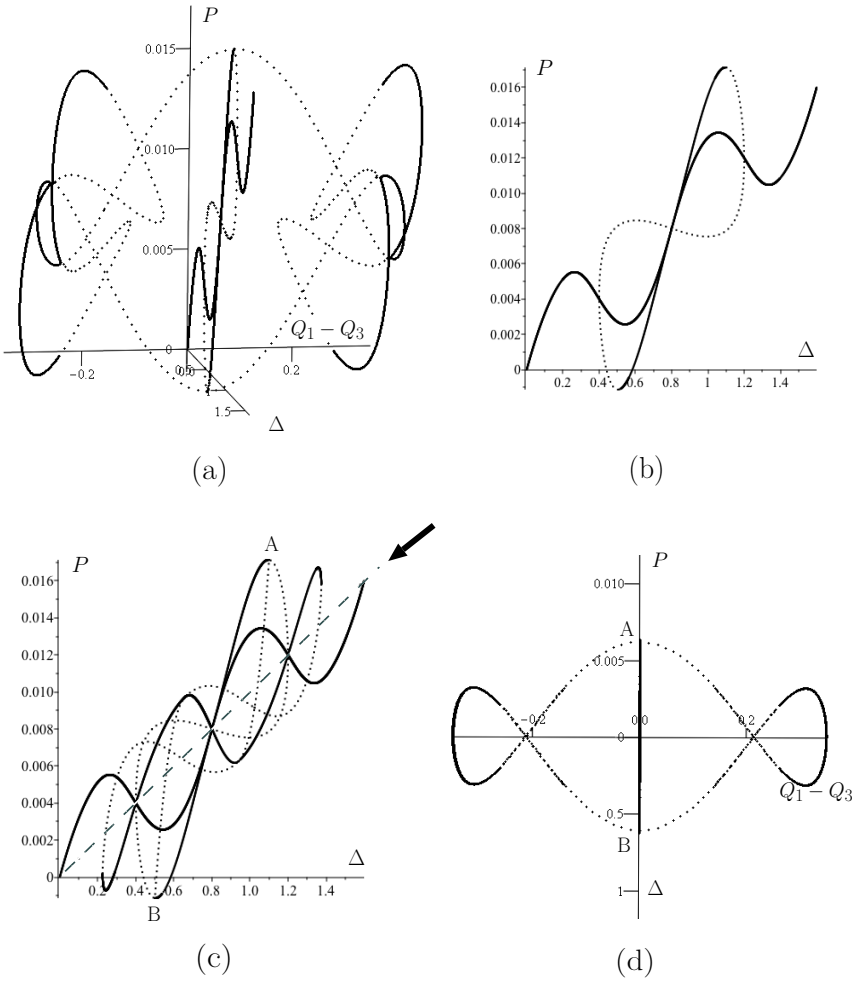

Figure 6. Response of a two-tier (three degree of freedom) system like that of Fig. 5 with $L = 1$, $h = 0.2$, $k = 0.5$ and $c = 0.02$. (a) Three dimensional plot of load P against its corresponding deflection Δ and the symmetry-breaking variable $(Q_1 - Q_3)$. (b) Symmetric solutions for which $Q_1 = Q_3$. (c) Projection of (a) onto the $P - \Delta$ plane. (d) Projection onto plane perpendicular to the direction of the arrow in (c).

extra contortions over and above those of Fig. 7(b), although the number of bifurcations into non-symmetric paths, marked again as B, remains at six.

4. Natural Loading Sequence

To this point we have concentrated on finding all possible equilibrium path of the system, stable and unstable, without indicating how a real system might behave on loading from zero. With the multiplicity of paths involved, a number of possibilities can arise. Of course only the stable paths can be followed, shown here in Fig.9(a) for the four tier model with the complete picture seen in Fig. 8.

On loading from zero, the system would initially follow the symmetric path up to the first bifurcation point A, where the deflections, load and end displacement are as given in Table 1. At this point, Q_2 and Q_4 have deflected considerably more than the other degrees of freedom, and the bifurcation implies an instability involving sudden increase in one of these with the other dropping back. From this point, under controlled end displacement, the system enters a

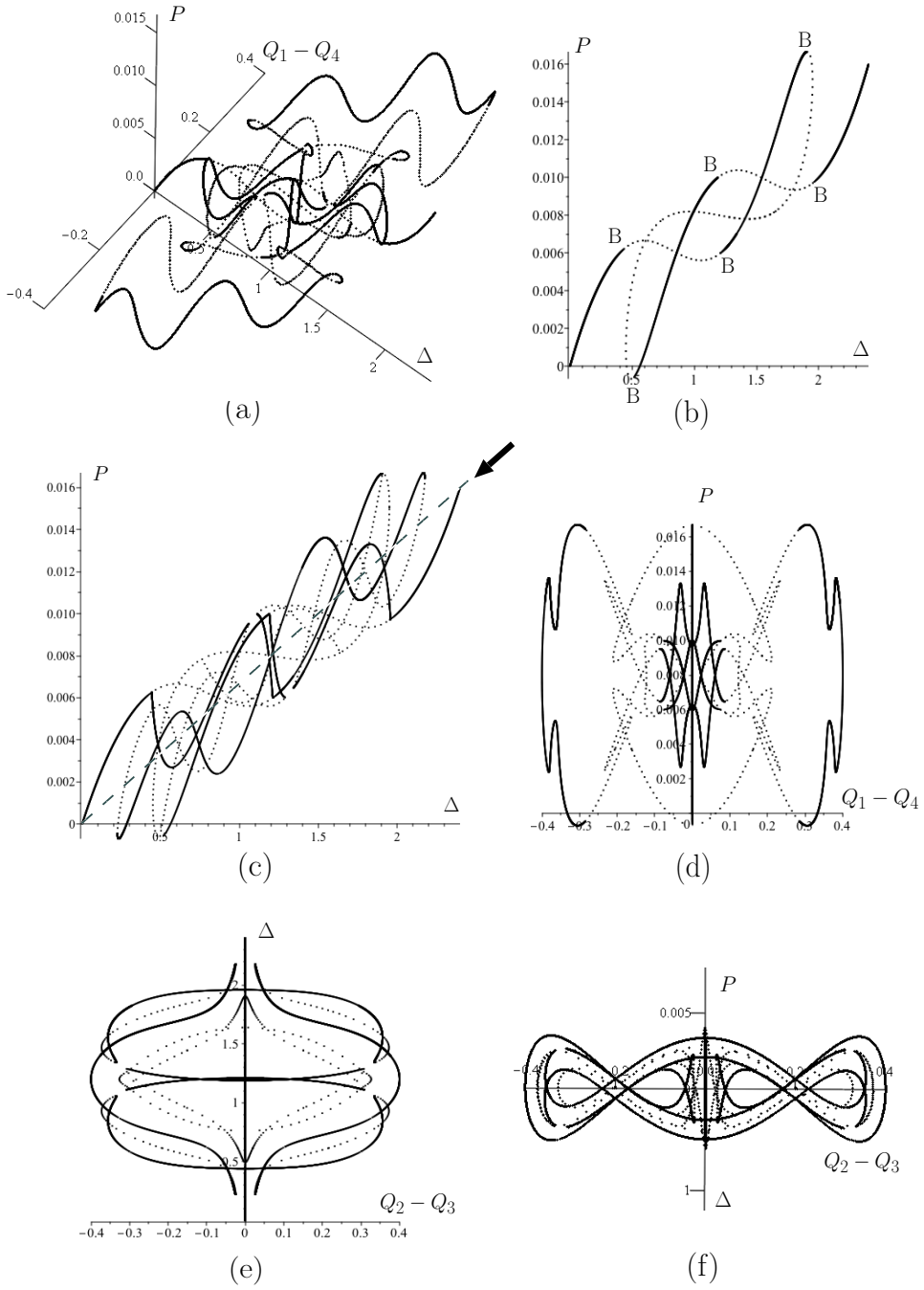

Figure 7. Response of a three-tier system of cells for $L = 1$, $h = 0.2$, $k = 0.5$ and $c = 0.02$. (a) Load P plotted against its corresponding deflection Δ and the symmetry-breaking variable $(Q_1 - Q_4)$. (b) Symmetric solutions for which $Q_1 = Q_4$ and $Q_2 = Q_3$. (c) Projection of (a) on to the $P - \Delta$ plane. (d) Projection of (a) on to the $P - (Q_1 - Q_4)$ plane. (e) Projection on to the $\Delta - (Q_2 - Q_3)$ plane. (f) Projection on to plane perpendicular to the direction of the arrow in (c).

dynamical phase with equilibrium equations alone not enough to determine behaviour. A sudden drop in load under constant Δ would mean that the system would end up on one of the three remaining stable paths. We would expect this to be the one shown as B in Fig.9(b), where either

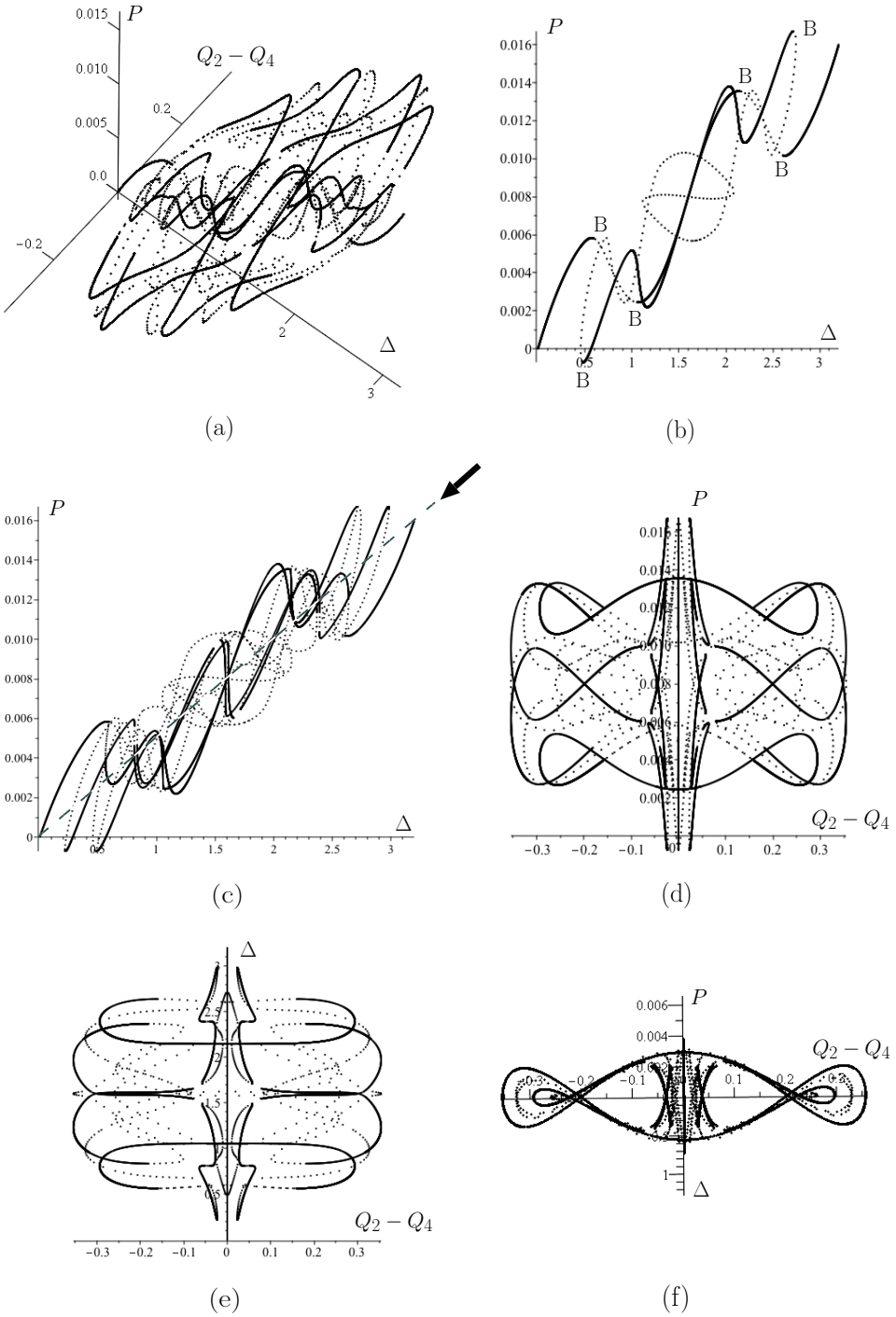

Figure 8. Response of a four-tier system of cells for $L = 1$, $h = 0.2$, $k = 0.5$ and $c = 0.02$. (a) Load P plotted against its corresponding deflection Δ and the symmetry-breaking variable $(Q_2 - Q_4)$. (b) Symmetric solutions for which $Q_1 = Q_5$ and $Q_2 = Q_4$. (c) Projection of (a) on to the $P - \Delta$ plane. (d) Projection of (a) on to the $P - (Q_2 - Q_4)$ plane. (e) Projection on to the $\Delta - (Q_2 - Q_4)$ plane. (f) Projection of (a) on to plane perpendicular to the direction of the arrow in (c).

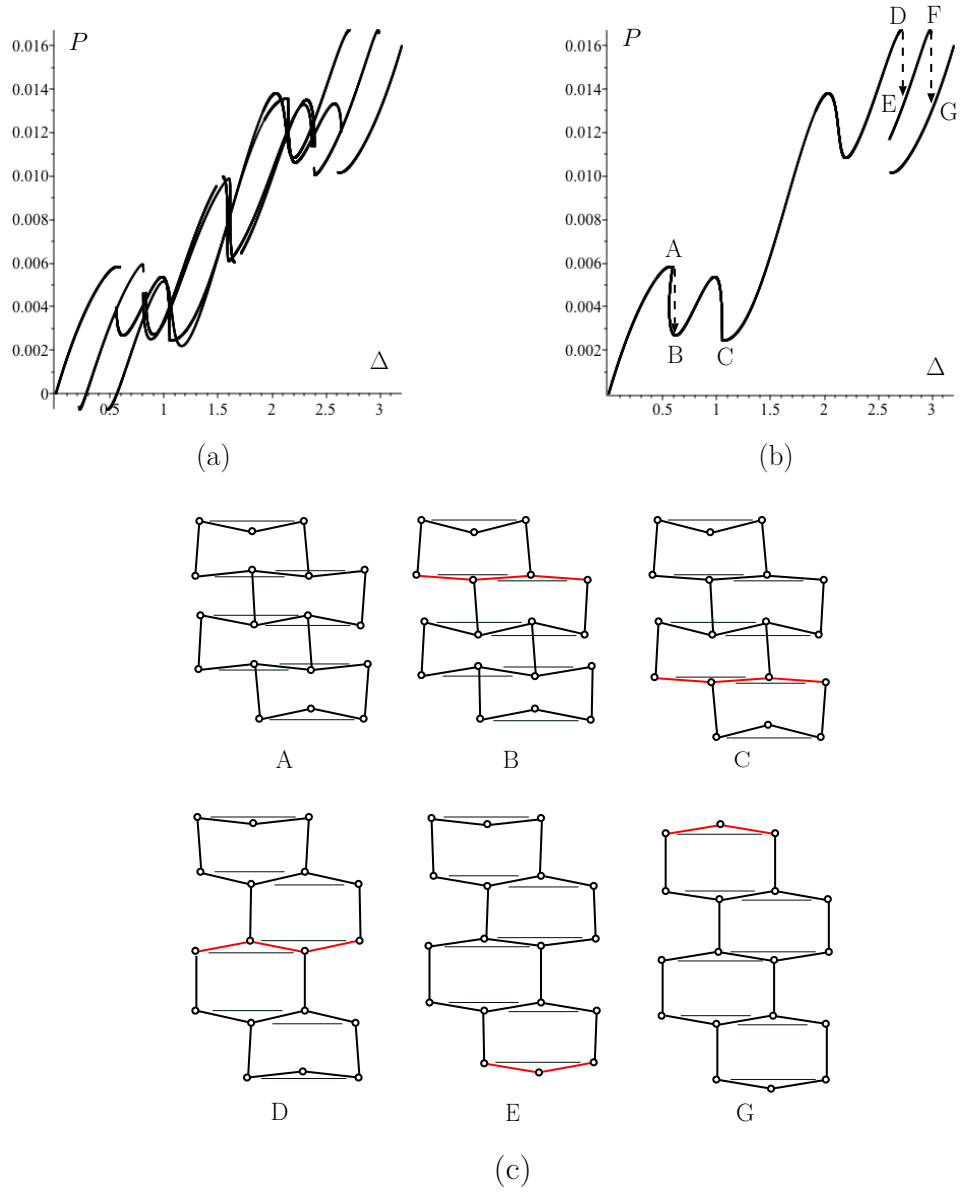

Figure 9. (a) Stable paths of Fig. 8. (b) Possible natural loading sequence under controlled end displacement. (c) Configurations at various positions on the natural loading path of (b).

Q_2 or Q_4 has passed through horizontal to turn negative, although the dynamics means that this is not necessarily guaranteed. Negative Q_2 or Q_4 means of course that the related row of arches has gone into its non-auxetic configuration. The other two possibilities involve in one case either Q_1 or Q_5 passing through horizontal to become non-auxetic, while the other is a symmetric configuration with both Q_1 and Q_5 non-auxetic.

Having restabilized in the asymmetric configuration of Fig. 9(b) at B, evolution under growing Δ then progresses stably, with deflection of the least displaced of Q_2 of Q_4 growing to meet that of its counterpart at bifurcation point C. Now, both the related rows of arches are in the non-auxetic state, and the path reconnects with the symmetric solution. Evolution then continues to progress in the symmetric configuration, during which Q_3 also passes into the non-auxetic state,

Position	Q_1	Q_2	Q_3	Q_4	Q_5	P	Δ
A	0.178	0.086	0.153	0.086	0.178	0.582e-2	0.594
B	0.213	-0.067	0.202	0.168	0.187	0.278e-2	0.594
C	0.216	-0.085	0.227	-0.085	0.216	0.245e-2	1.054
D	0.102	-0.230,	-0.201	-0.230	0.102	0.167e-1	2.718
E	0.166	-0.210	-0.168	-0.172	-0.186	0.131e-1	2.718
F	-0.203	-0.205	-0.202	-0.228	0.089	0.166e-1	2.985
G	-0.185	-0.168	-0.171	-0.168	-0.185	0.129e-1	2.985

Table 1. Deflections, loads and end displacements at various positions on the load path of Fig. 9.

until bifurcation point D is reached. Here there would then be a further dynamic snap under constant Δ to one of the lower equilibrium states, depicted here as the asymmetric configuration E, where all but one of the arches have now become non-auxetic. Progress is then shown along the aysmmetric path to the final instability F, where a dynamical snap would drop the system onto the symmetric state with all arches non-auxetic. Depending on the dynamics, it might however be possible for this path to be reached directly from D. Displacement finally continues to the point where $\Delta = 3.2$ and $Q_i = -0.2$ for all i, which is considered to be the end of the transition between auxetic and non-auxetic phases.

In summary therefore, the path of Fig. 9(b) involves a fluctuating sequence in which the rows of arches pass sequentially from auxetic to non-auxetic states, in the order Q_2 (or Q_4), Q_4 (or Q_2), Q_3, Q_1 (or Q_5), and finally Q_5 (or Q_1), involving a total of three dynamic snaps. Configurations from a typical such sequence are shown in Fig. 9(c).

5. Emergent Stiffness and Modulus

We now compare the responses of the one, two, three and four-tier systems, as seen in Figs. 3 and 6 to 8, and by inference attempt to predict behaviour for larger cellular systems. All responses show a wide range of local stiffness with both positive and negative values. However a general trend is indicated by the dashed lines of Figs. 3(b) and 6(c) to 8(c), which is generally upwards with an underlying positive stiffness. The response oscillates about this line, with an increasing number of fluctuations as the number of tiers, n, increases. As the length of the sample also increases with n, interest then naturally turns to frequency of oscillation as measured by the number of fluctuations per unit length. The fluctuations collapse onto the dashed lines as $h \to 0$, leading us to describe the slope as the *emergent stiffness* and the product of this slope and the length of the sample (number of tiers) as the *emergent modulus*.

This information is summarized in Table 2, which lists also the number of fluctuations over the

Tiers (n)	Fig	Height (h)	Transition Length	Emergent stiffness	Emergent modulus	Fluctuations	Fluctuation frequency
1	3(b)	0.2	0.8	0.02	0.02	4	5
2	6(c)	0.2	1.6	0.01	0.02	16	10
3	7(c)	0.2	2.4	0.0067	0.02	30	12.5
4	8(c)	0.2	3.2	0.005	0.02	60	18.75
4	10(b)	0.1	1.6	0.005	0.02	16	10

Table 2. Emergent modulus and evidence of additional complexity with increasing number of tiers.

transition length shown in the figures, as measured by the number of times an equilibrium path crosses the appropriate dashed line. This count is taken from the load to corresponding plots of 3(b) and 6(c) to 8(c) in which mirror-image responses appear identical, so the actual number of

crossings would be greater than the listed value. We see that the emergent modulus, defined by $E =$ effective stress/effective strain, where effective stress = total load/width and effective strain = Δ/effective length, computes to the same value for all n and arch heights h. Thus if n is increased to a large number for a given transition length by dropping the value of h, the effective Young's modulus of the resulting material would approach this value. This trend is demonstrated by the four tier plots of Fig. 10 with the reduced value of $h = 0.1$. This is the same result as would

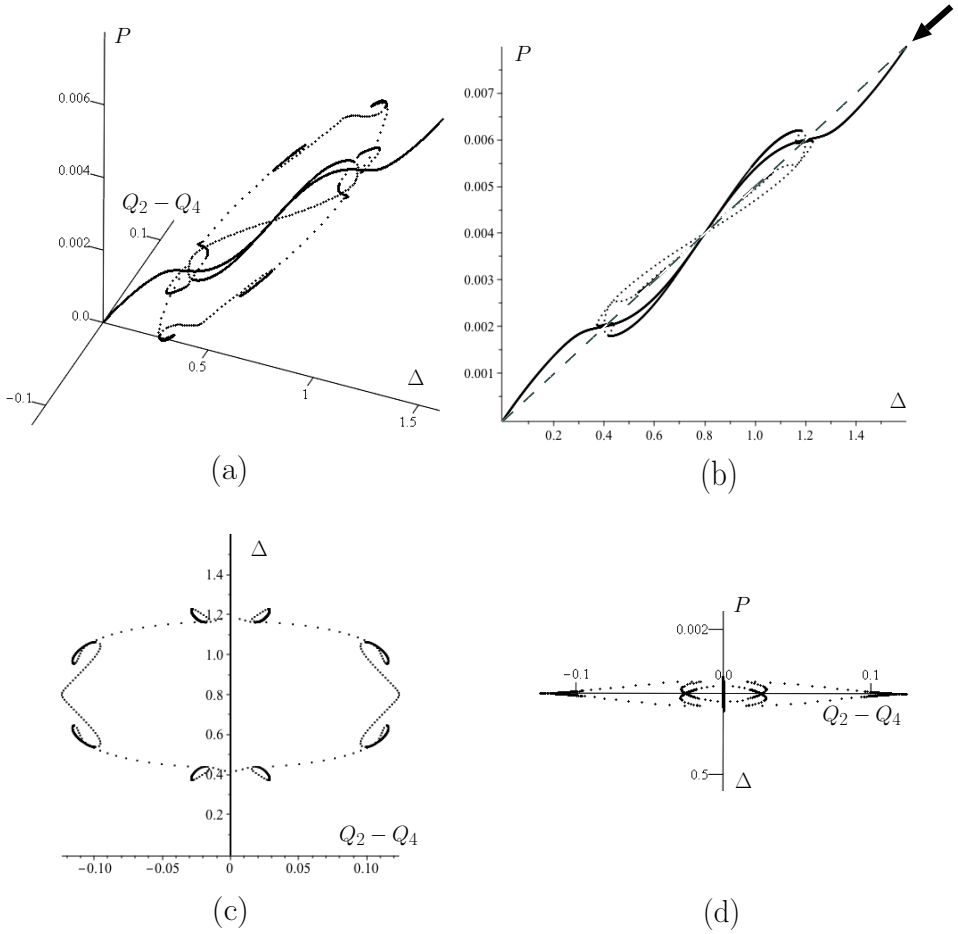

Figure 10. Response of a four-tier system of cells with shallow arch height. $L = 1$, $h = 0.1$, $k = 0.5$ and $c = 0.02$. (a) Load P plotted against its corresponding deflection Δ and the symmetry-breaking variable $(Q_2 - Q_4)$. (b) Projection of (a) on to the $P - \Delta$ plane. (c) Projection on to the $\Delta - (Q_2 - Q_4)$ plane. (f) Projection of (a) on to plane perpendicular to the direction of the arrow in (b).

have been obtained from the linear coupling springs alone, in the absence of all nonlinear effects resulting from the arch components. Meanwhile, for a given h, the frequency of fluctuation, as measured by fluctuations per unit length, effectively doubles with each additional tier. We can thus conclude that the complexity becomes significantly more severe with increasing n.

6. Concluding Remarks

It has successfully been demonstrated that the transition stage between auxetic and non-auxetic phases of a particular cellular model has a complex characteristic, with the response fluctuating

in both load and corresponding deflection of the load. A multiple number of cells in the direction orthogonal to that of the loading, and up to four tiers of cells in the direction of loading, are used to demonstrate the increasing complexity of the response as the number of cells is increased. It is suggested that, if the phase transition length is maintained constant by increasing the number of cells while reducing the effective local arch height, the fluctuations would diminish in amplitude in relation to the global scale, and the response would crush down onto the *emergent stiffness* of the material as a whole.

It turns out that for this particular model, the emergent stiffness is the same as the stiffness of the linear coupling springs alone, in the absence of the interior arch components that give rise to the nonlinear effects and consequent auxetic response. Although this is the case for the simple system given here, in a more realistic auxetic setting the contributions may not be quite so obvious. The possibility of determining an emergent stiffness for a more practical auxetic material remains an interesting and open question.

It should be noted that contributions to end displacement due to inclination of the initially-vertical rods at the sides of cells is ignored in this formulation. This would normally be regarded as a second-order effect, but as it accumulates across the width of a sample it should in fact be included. The effect diminishes as the rods get longer and the arch height diminishes, so we can regard the formulation as justified in the same limit of emergent stiffness and modulus as described above. It could of course be included analytically, but that would tend to complicate matters without providing any extra insight.

This paper has focused on the conceptual idea of introducing pin-jointed lattices, and exploring the resulting complex mechanics such structures exhibit. However from a practical side, one might naturally ask how could such a material be manufactured. Of course a prototype model could be constructed from MECCANO^{TM} like members and springs. More sophisticated possibilities could exist, where the material was 3D printed as a heterogenous material, members as a stiff material, and springs and joints as compliant elastomer. In this case the joints would carry a small moment, yet if the size of the joints and material were chosen carefully the resulting mechanics of the material would be little effected from that studied here. This is a future avenue of research.

We note finally that apparent auxetic behaviour is not only found in re-entrant structures. Examples of similar behaviour can appear in systems with negative-stiffness inclusions [17] or components [18], and rotating spherical particles in a granular medium [19].

Data Accessibility. This article has no additional data.

Authors' Contributions. This piece of work represents an equal collaboration in all aspects of the paper.

Competing Interests. There are no competing interests.

Funding. This work was supported by The Alan Turing Institute under the EPSRC grant EP/N510129/1.

Acknowledgements. There are no acknowledgements in this paper.

References

1. Evans KE, Alderson A, 2000 Auxetic materials: functional materials and structures from lateral thinking! *Advanced Materials* **12**(9) 617–628.
2. Evans KE, Alderson KL, 2000 Auxetic materials: the positive side of being negative, *Engineering Science and Education Journal* **9**(4) 148–154.
3. Fu MH, Chen Y, Hu LL. 2017 Bilinear elastic characteristic of enhanced auxetic honeycombs. *Composite Structures* **175** 101–110.
4. Evans KE, Nkansah MA, Hutchinson IJ, Rogers SC. 1991 Molecular network design, *Nature* **353** 124.
5. Lakes, RS, 1987 Foam structures with a negative Poisson's ratio, *Science*, **235** 1038–1040.
6. Bertoldi K, Reis PM, Willshaw S and Mullin T. 2010 Negative poisson's ratio behaviour induced by an elastic instability. *Advanced Materials* **22** 361–366.
7. Overvelde JTB, Shan S and Bertoldi K. 2012 Compaction through buckling in 2D periodic, soft and porous structures: effect of pore shape. *Advanced Materials* **24** 2337–2342.

8. Yang W, Li ZM, Shi W, Xie BH, Yang MB. 2004 Review on auxetic materials. *J. Mater. Sci.* **39** 3269–3279.
9. Huang, J, Zhang, Q, Scarpa, F, Liu, Y and Leng, J. 2017 In-plane elasticity of a novel auxetic honeycomb design. *Composites Part B: Engineering*, **110** 72–82.
10. Hunt GW, Peletier MA, Champneys AR, Woods PD, Wadee MA, Budd CJ, Lord GJ. 2000 Cellular buckling in long structures. *Nonlinear Dynamics* **21**(1) 3–29.
11. Murphy KD, Hunt GW, Almond DP. 2006 Evidence of emergent scaling in mechanical systems. *Philos. Mag.* **86** 3325–3338.
12. Almond DP, Budd CJ, Freitag MA, Hunt GW, McCullen NJ, Smith ND. 2013. The origin of power-law emergent scaling in large binary networks. *Physica A* **392** 1004–1027.
13. Thompson JMT, Hunt GW. 1984 *Elastic instability phenomena*. Wiley, Chichester.
14. Thompson JMT, Hunt GW. 1973 *A general theory of elastic stability*. Wiley, London.
15. *Maple (2017). Maplesoft, a division of Waterloo Maple Inc., Waterloo, Ontario*.
16. Hunt GW. 1989 Bifurcation of structural components. *Proc. Instn. Civ. Engrs. Part 2* **87** 443–467.
17. Dyskin, AV, Pasternak E. 2012. Elastic composite with negative stiffness inclusions in antiplane strain. *Intern. J. Engineering Sci.* **58** 45–56.
18. Esin M, Pasternak E, Dyskin, AV. 2016. Stability of chains of oscillators with negative stiffness normal, shear and rotational springs. *Intern. J. Engineering Sci.* **108** 16–33.
19. Dyskin, AV, Pasternak E. 2012. Mechanical effect of rotating non-spherical particles on failure in compression. *Philos. Mag.* **92** 3451–3473.